

# Large enhancement of nonlinear terahertz absorption in intrinsic GaAs by plasmonic nano antennas

Young-Gyun Jeong,<sup>1,2,a)</sup> Michael J. Paul,<sup>2,a)</sup> Seung-Hyun Kim,<sup>3</sup> Ki-Ju Yee,<sup>3</sup> Dai-Sik Kim,<sup>1,b)</sup> and Yun-Shik Lee<sup>2,b)</sup>

<sup>1</sup>Department of Physics and Astronomy and Center for Subwavelength Optics, Seoul National University, Seoul 151-747, South Korea

<sup>2</sup>Department of Physics, Oregon State University, Corvallis, Oregon 97331-6507, USA

<sup>3</sup>Department of Physics and GRAFT, Chungnam National University, Daejeon 305-764, South Korea

(Received 6 August 2013; accepted 6 October 2013; published online 22 October 2013)

We demonstrate remarkably strong nonlinear terahertz (THz) effects in an intrinsic GaAs wafer patterned with a nanometer-width slot antenna array. The antenna near-field reaches 20 MV/cm due to the huge field enhancement in the plasmonic nano-structure (field enhancement factor,  $\alpha \cong 50$ ). The THz fields are strong enough to generate high density free carriers ( $N_e > 10^{17} \text{ cm}^{-3}$ ) via interband excitations associated with impact ionizations and thus to induce large absorption of the THz radiation ( $>35\%$ ). The nonlinear THz interactions take place in the confined region of nanometer-scale layer adjacent to the antenna. © 2013 AIP Publishing LLC.  
[\[http://dx.doi.org/10.1063/1.4826272\]](http://dx.doi.org/10.1063/1.4826272)

Terahertz (THz) spectroscopy of carrier dynamics in semiconductors is of great interest not only for understanding the fundamental physical processes such as many-body Coulomb interactions and carrier-phonon scattering but also for developing high-speed electronic devices.<sup>1</sup> In particular, recent technical advances in high-power THz pulse generation have opened up new opportunities to explore high-field electron transport and non-equilibrium carrier distribution in semiconductors.<sup>2,3</sup> The interaction of strong THz pulses with semiconductors results in pronounced nonlinear THz responses in that hot electrons driven by intense THz fields undergo scattering processes of different kinds such as intervalley scattering and impact ionization.<sup>4–6</sup> The nonlinear THz properties are governed by various physical parameters such as bandgap energy, temperature, carrier type, carrier density, and doping level.

GaAs, the material of interest in this study, is of great importance because of the fundamental interests in high-frequency carrier dynamics as well as the applications to ultra-high speed electronics.<sup>7–10</sup> The previous studies on n-type GaAs with the THz fields in the range of  $\sim 100 \text{ kV/cm}$  show that the electrons driven into high momentum states by the THz fields undergo distinctive intraband processes such as intervalley scattering,<sup>11,12</sup> coherent ballistic transport,<sup>13,14</sup> and effective mass anisotropy.<sup>15</sup> It is notable that the intervalley scattering from initial conduction band valley ( $\Gamma$  valley) to side valleys (L valley or X valley) is considered to be the dominant mechanism for the THz induced transparency in the n-type GaAs samples of the electron density around  $10^{15}–10^{17} \text{ cm}^{-3}$  due to the lower electron mobility in the side valleys. In the higher field regime beyond 1 MV/cm, THz fields may produce extreme nonlinear effects involving interband transitions in GaAs, while the THz photon energy is several hundred times lower than the bandgap energy.<sup>6,16</sup>

For example, it has been reported that THz excitations generated photoluminescence in GaAs quantum wells (QWs), which was associated with carrier multiplication through a series of impact ionizations.<sup>6</sup>

In this letter, we demonstrate that the field enhancement in plasmonic THz nano-antennas raises the near-field amplitude up to 20 MV/cm and hence gives rise to the onset of extraordinary nonlinear THz absorption in intrinsic GaAs associated with carrier generation by THz excitations. THz photon energy is orders-of-magnitude smaller than the bandgap energy, yet the THz electric fields are so strong that they create free carriers in the conduction band via interband transitions. We used the undoped samples to suppress intraband processes such as intervalley scattering. Nonlinear optical processes in metal-semiconductor hybrid nanostructures hold potential for practical applications such as active switching devices, modulators, and frequency filters.<sup>17–19</sup> Especially, nanometer-width slot antenna structures, which are simple and easy to fabricate, can make huge field enhancement more than 100 times at the resonance frequency.<sup>20–23</sup> The field enhancement and consequent nonlinear optical effects in nano-slot antenna/semiconductor composites give rise to effective dielectric constant modulation.<sup>19,24</sup> We exploit the field enhancement in THz nano-slot antennas to obtain intense THz fields up to 20 MV/cm and to investigate high-field transient carrier dynamics in intrinsic GaAs.

We fabricated nano-slot-antenna arrays on a 500- $\mu\text{m}$ -thick, single crystal intrinsic (100) GaAs wafer, using an electron beam lithography technique. The resistivity of GaAs wafer is  $(1.0–2.9) \times 10^8 \Omega \text{ cm}$ , the mobility is  $(5.5–6.2) \times 10^3 \text{ cm}^2/\text{V s}$ , and the average carrier density is  $\sim 7 \times 10^6 \text{ cm}^{-3}$  at room temperature. Figure 1(a) illustrates the nano-antenna/GaAs composite design: each antenna is 60  $\mu\text{m}$  long ( $l_1$ ) and 200 nm wide ( $w$ ), which is resonant at 0.9 THz. The antenna array is a negative structure in a 100-nm-thick-gold/3-nm-thick-Ti-adhesion layer on top of the GaAs wafer. In order to optimize the field enhancement at the resonance frequency and to avoid coupling effects among neighboring antennas, the periodicity

<sup>a)</sup>Y. G. Jeong and M. J. Paul contributed equally to this work.

<sup>b)</sup>Authors to whom correspondence should be addressed. Electronic addresses: dsk@phya.snu.ac.kr and leeys@physics.oregonstate.edu

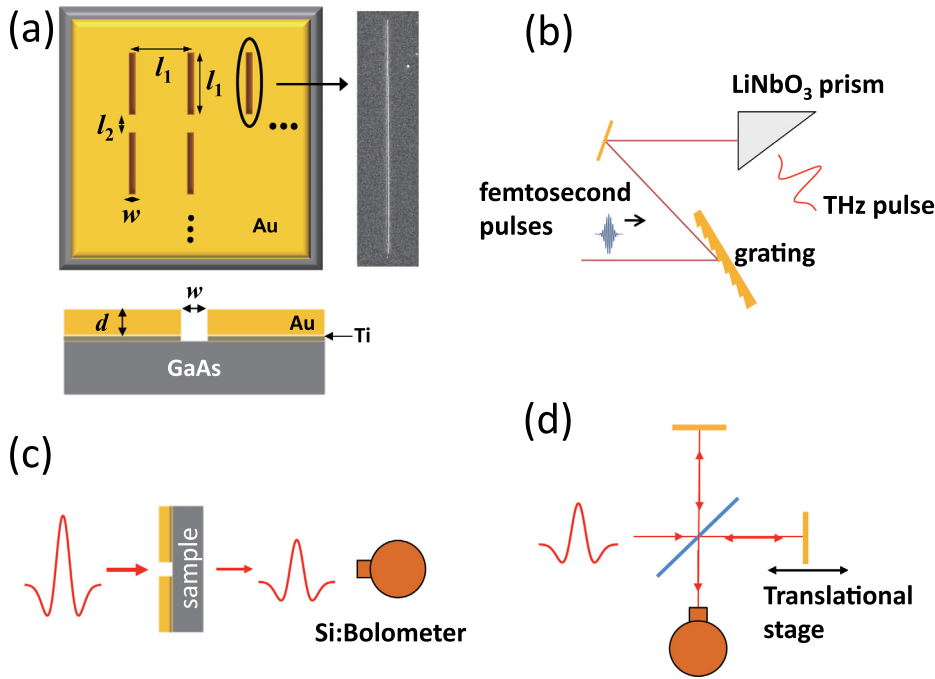


FIG. 1. (a) Nano-slot-antenna-array-patterned GaAs sample: the dimensions are  $l_1 = 60 \mu\text{m}$ ,  $l_2 = 10 \mu\text{m}$ , and  $w = 200 \text{nm}$ . The thickness of the gold layer is  $d = 100 \text{nm}$  and the adhesion titanium layer is  $3 \text{nm}$ . A SEM image of a single nano-antenna is shown. (b) Schematic of the high-power THz pulse generation setup with a lithium niobate prism. (c) Total transmitted power measurement with a liquid-helium-cooled silicon-bolometer. (d) Michelson interferometer setup for frequency spectrum measurement.

of the antenna array in the length direction ( $70 \mu\text{m}$ ) and width direction ( $60 \mu\text{m}$ ) is the same scale with the antenna length ( $l_1$ ).<sup>25</sup> The total array area,  $2 \text{mm}$  by  $2 \text{mm}$ , is substantially larger than the incident THz beam size at the focal plane ( $400\text{-}\mu\text{m}$  diameter). We generate strong THz pulses via tilted-pulse-front optical rectification in a  $\text{LiNbO}_3$  prism using femtosecond pulses (pulse duration,  $120 \text{fs}$ ; wavelength,  $800 \text{nm}$ ) from a  $1\text{-kHz}$  Ti:Sapphire regenerative amplifier (Fig. 1(b)).<sup>2</sup> The field amplitude of the broadband THz pulses (central frequency,  $0.9 \text{THz}$ ; bandwidth,  $0.8 \text{THz}$ ) reaches  $500 \text{kV/cm}$  at an optical pulse energy of  $0.8 \text{mJ}$ . We measured the transmitted THz pulses using a liquid-helium-cooled silicon-bolometer to obtain either spectrally integrated total transmitted power (Fig. 1(c)) or transmission frequency spectra via Michelson interferometry (Fig. 1(d)). We carried out the THz transmission measurements on the nano-antenna/GaAs composite as well as a bare GaAs wafer for comparison.

The experimental results for the bare GaAs sample are shown in Fig. 2, where the THz transmission is the transmitted power through the sample divided by the transmitted power in the absence of a sample. Figure 2(a) shows the transmission as a function of the THz field amplitude, when the field is aligned along (110) direction. We also obtained nearly identical results in (100) direction. The THz transmission undergoes only a small decrease up to  $150 \text{kV/cm}$  and becomes flattened, which is independent of the field direction relative to the crystal axis. The normalized transmission decrease ( $\Delta T/T_0$ ) is less than  $1.5\%$  in this field range of  $E_{\text{THz}} < 600 \text{kV/cm}$ . Though the increase in THz absorption implies free carrier generation by the THz excitation, it is hard to expect drastic carrier density changes in bare GaAs. Figure 2(b) shows the electron density  $N_e$  estimated from the free-carrier absorption coefficient,

$$\gamma(E_{\text{THz}}) = \frac{e\mu_e}{c\epsilon_0 n_G} N_e(E_{\text{THz}}) = \frac{1}{l_G} \ln \frac{T_0}{T(E_{\text{THz}})}, \quad (1)$$

where  $T_0 (=0.512)$  is the linear THz transmission of the GaAs wafer,  $l_G (=500 \mu\text{m})$  is the wafer thickness,  $e$  is the electron charge,  $\mu_e (\cong 6 \times 10^3 \text{cm}^2/\text{V s})$  is the mobility,  $c$  is the speed of light, and  $n_G (=3.6)$  is the GaAs refractive index

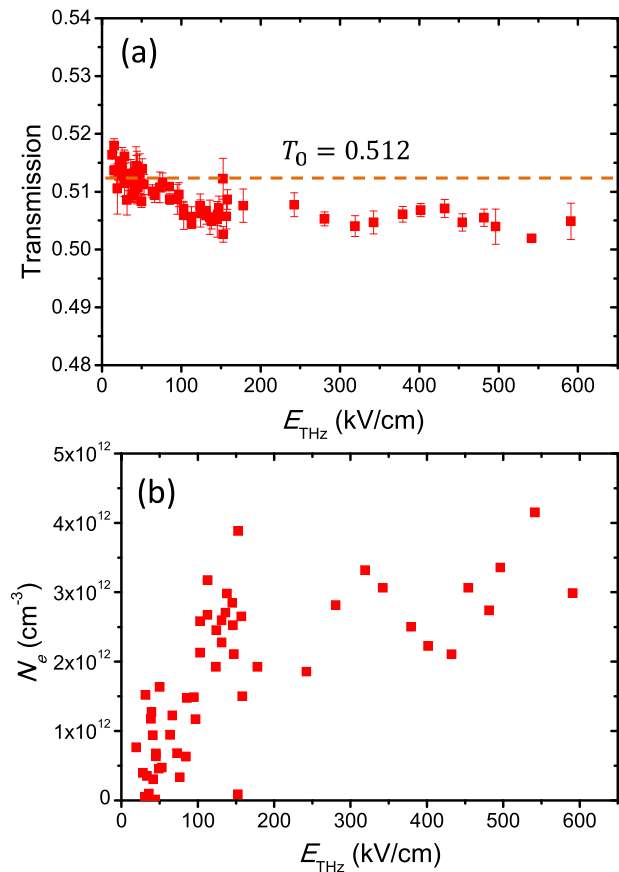


FIG. 2. Bare GaAs wafer: (a) spectrally integrated THz transmission vs. field amplitude for the field aligned along (110) direction. The dashed line at  $0.512$  indicates the low-field transmission of the GaAs wafer ( $n_G = 3.6$ ) including internal reflections. (b) Estimated free carrier density vs. THz field amplitude.

in the THz region. The electron density gradually builds up to  $3 \times 10^{12} \text{ cm}^{-3}$  and becomes saturate above 150 kV/cm. The THz field lower than 600 kV/cm is too weak to induce interband transitions either by Zener tunneling or by impact ionization.<sup>6</sup> We speculate that the THz excitations free up electrons trapped in shallow impurity states.

Figure 3 shows the experimental results for the nano-antenna-array-patterned GaAs sample. For the transmitted power measurements as shown in Fig. 3(a), the transmission decreases by more than 35% over a factor-of-ten increase in the field strength. The significant change in the THz transmission implies that the strong THz fields generate a substantially large number of free carriers via interband transitions. As depicted in Fig. 3(b), the carrier density is enhanced by a factor of  $\sim 10^5$  compared to that in bare GaAs

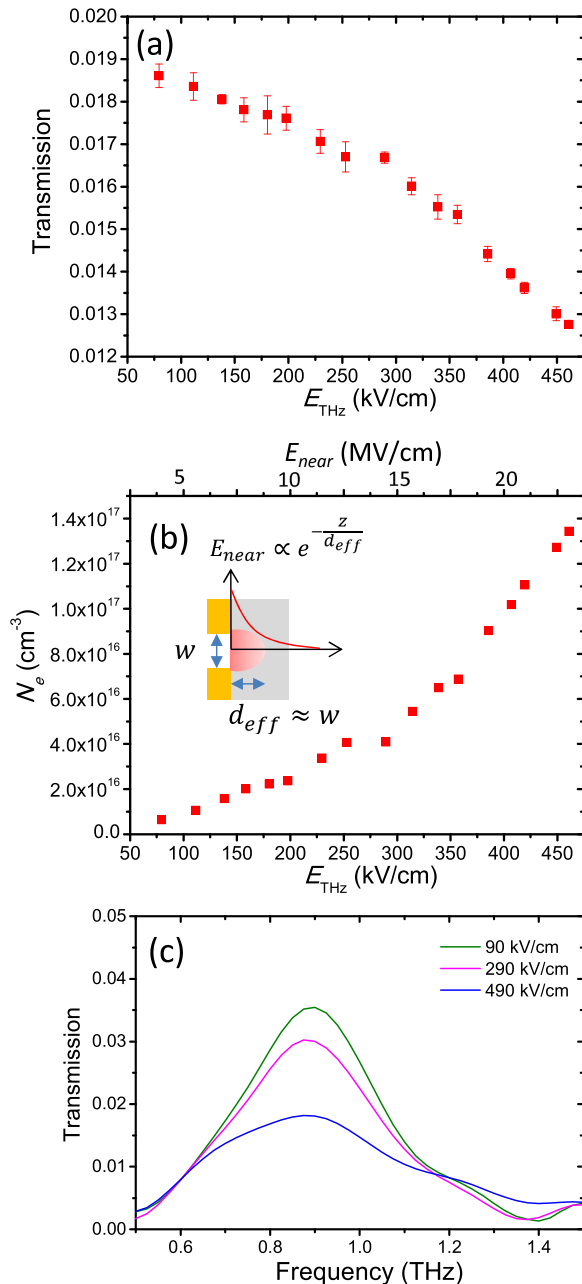


FIG. 3. Nano-antenna/GaAs composite: (a) spectrally integrated THz transmission vs. field amplitude. (b) Free carrier density vs. THz field. (c) Transmission spectra at 90, 290, and 490 kV/cm.

for the same input intensities. The transmission spectra shown in Fig. 3(c) reveal the antenna resonance at 0.9 THz and also demonstrate large increase in absorption at high THz fields. The transmission reduction at 490 kV/cm at the resonance frequency compared to that at 90 kV/cm reaches 50%. Furthermore, the spectral broadening indicates the increase of conductivity and thus free-carrier generation by the THz fields.

As the first step of a phenomenological analysis, we calibrate the THz field amplitude at the nano-slot (the near field amplitude,  $E_{\text{near}}$ ) using the field enhancement factor of the nano-antenna structure<sup>20</sup>

$$\alpha = \frac{|E_{\text{near}}|}{|E_{\text{THz}}|} = \frac{1}{\beta} \left| \frac{E_{\text{far}}}{E_{\text{THz}}} \right| \cong 50, \quad (2)$$

where the antenna coverage ratio  $\beta$  is 1/350 for this sample. The ratio of the far-field to the incident field amplitude ( $E_{\text{far}}/E_{\text{THz}}$ ) is obtained from the observed THz transmission at low intensities (the transmission is 1.9% and the ratio of the pulse duration of transmitted radiation to that of incident radiation is 2.3). The near-field amplitude exponentially decays along the direction perpendicular to the antenna/GaAs interface, i.e.,  $E_{\text{near}}(z) \approx E_{\text{near}}(0)e^{-z/w}$ , which indicates that the large nonlinear THz absorption arises mostly in the confined region of the nanometer-scale layer,  $d_{\text{eff}} \approx w = 200 \text{ nm}$ .<sup>19</sup>

The effective thickness is a mere 1/1500th of the wafer thickness, meaning that the nonlinear effects in the nano-antenna structure are several orders of magnitude stronger than those in bare GaAs. As a first-order approximation to analyze the nonlinear THz absorption, we treat the nanometer-scale layer as a conducting thin film and apply the thin-film Fresnel formula to obtain the THz induced conductivity from the nonlinear transmission measurements. The THz-field induced conductivity is expressed as a function of the normalized nonlinear transmission,  $T_{\text{rel}}(E_{\text{THz}}) = T(E_{\text{THz}})/T_0$ :

$$\sigma(E_{\text{THz}}) = \frac{n_G + 1}{Z_0 d_{\text{eff}}} \left[ \frac{1}{\sqrt{T_{\text{rel}}(E_{\text{THz}})}} - 1 \right], \quad (3)$$

where  $Z_0$  ( $= 376.7 \ \Omega$ ) is the vacuum impedance. We estimate the free electron density from the conductivity, applying the mobility-conductivity relation:  $N_e(E_{\text{THz}}) = \sigma(E_{\text{THz}})/e\mu_e$ . The calculated electron density is shown in Fig. 3(b) as a function of the incident THz field amplitude (the near field amplitude is scaled on the top axis). This simple approximation underestimates the carrier density because the electron mobility decreases as the carrier density increases in the high density regime. Nevertheless, the estimated carrier density exceeds  $10^{17} \text{ cm}^{-3}$  for  $E_{\text{THz}} > 400 \text{ kV/cm}$ . In this high field regime, the most probable carrier generation mechanism is the carrier multiplication by impact ionization.<sup>6,26,27</sup> The initial electron density in the conduction band is  $N_0 \sim 7 \times 10^6 \text{ cm}^{-3}$ , and thus the number of impact ionizations,  $n_I = \log_2(N_e/N_0)$ , is estimated as 33–37 for  $E_{\text{near}} = 5\text{--}20 \text{ MV/cm}$ . An alternative carrier generation mechanism is Zener tunneling, which would be appreciable above  $\sim 10 \text{ MV/cm}$ .<sup>28</sup> More detailed studies are desirable to unveil the microscopic origins of the THz excited carriers.

In summary, our experimental study demonstrates that strong THz pulses induce nonlinear THz absorption in intrinsic GaAs. The huge field enhancement in the nano-antenna array,  $\alpha \cong 50$ , produces THz fields exceeding 20 MV/cm adjacent to the antennas. The strong fields induce remarkably large THz absorption ( $>35\%$ ) by generating free carriers of high density ( $>10^{17} \text{ cm}^{-3}$ ) via interband excitations associated with impact ionizations. The experimental scheme exploiting the nano-antenna field enhancement is versatile for nonlinear THz spectroscopy and can be applied to a variety of materials.

This work was supported by the National Science Foundation (DMR-1063632) and the National Research Foundation of Korea (NRF) grant funded by the Korea government (MSIP) (2008-0061906, 2005-0093838) (GRL, K20815000003).

- <sup>1</sup>R. Ulbricht, E. Hendry, J. Shan, T. F. Heinz, and M. Bonn, *Rev. Mod. Phys.* **83**, 543 (2011).  
<sup>2</sup>K. Kawase, M. Sato, T. Taniuchi, and H. Ito, *Appl. Phys. Lett.* **68**, 2483 (1996).  
<sup>3</sup>J. Hebling, Y. Ka-Lo, K. A. Nelson, and M. C. Hoffmann, *IEEE J. Sel. Top. Quantum Electron.* **14**, 345 (2008).  
<sup>4</sup>I. C. Ho and X. C. Zhang, *Appl. Phys. Lett.* **98**, 241908 (2011).  
<sup>5</sup>M. C. Hoffmann, J. Hebling, H. Y. Hwang, K.-L. Yeh, and K. A. Nelson, *Phys. Rev. B* **79**, 161201 (2009).  
<sup>6</sup>H. Hirori, K. Shinokita, M. Shirai, S. Tani, Y. Kadoya, and K. Tanaka, *Nat. Commun.* **2**, 594 (2011).  
<sup>7</sup>P. Gaal, K. Reimann, M. Woerner, T. Elsaesser, R. Hey, and K. H. Ploog, *Phys. Rev. Lett.* **96**, 187402 (2006).  
<sup>8</sup>F. H. Su, F. Blanchard, G. Sharma, L. Razzari, A. Ayesheshim, T. L. Cocker, L. V. Titova, T. Ozaki, J. C. Kieffer, R. Morandotti, M. Reid, and F. A. Hegmann, *Opt. Express* **17**, 9620 (2009).  
<sup>9</sup>G. Sharma, I. Al-Naib, H. Hafez, R. Morandotti, D. G. Cooke, and T. Ozaki, *Opt. Express* **20**, 18016 (2012).

- <sup>10</sup>Y. Shi, Q.-I. Zhou, C. Zhang, and B. Jin, *Appl. Phys. Lett.* **93**, 121115 (2008).  
<sup>11</sup>J. Hebling, M. C. Hoffmann, H. Y. Hwang, K.-L. Yeh, and K. A. Nelson, *Phys. Rev. B* **81**, 035201 (2010).  
<sup>12</sup>D. Turchinovich, J. M. Hvam, and M. C. Hoffmann, *Phys. Rev. B* **85**, 201304 (2012).  
<sup>13</sup>W. Kuehn, P. Gaal, K. Reimann, M. Woerner, T. Elsaesser, and R. Hey, *Phys. Rev. Lett.* **104**, 146602 (2010).  
<sup>14</sup>P. Bowlan, W. Kuehn, K. Reimann, M. Woerner, T. Elsaesser, R. Hey, and C. Flytzanis, *Phys. Rev. Lett.* **107**, 256602 (2011).  
<sup>15</sup>F. Blanchard, D. Golde, F. H. Su, L. Razzari, G. Sharma, R. Morandotti, T. Ozaki, M. Reid, M. Kira, S. W. Koch, and F. A. Hegmann, *Phys. Rev. Lett.* **107**, 107401 (2011).  
<sup>16</sup>K. Fan, H. Y. Hwang, M. Liu, A. C. Strikwerda, A. Sternbach, J. Zhang, X. Zhao, X. Zhang, K. A. Nelson, and R. D. Averitt, *Phys. Rev. Lett.* **110**, 217404 (2013).  
<sup>17</sup>H.-T. Chen, W. J. Padilla, J. M. O. Zide, A. C. Gossard, A. J. Taylor, and R. D. Averitt, *Nature* **444**, 597 (2006).  
<sup>18</sup>H.-T. Chen, W. J. Padilla, M. J. Cich, A. K. Azad, R. D. Averitt, and A. J. Taylor, *Nat. Photon.* **3**, 148 (2009).  
<sup>19</sup>A. Degiron, J. J. Mock, and D. R. Smith, *Opt. Express* **15**, 1115 (2007).  
<sup>20</sup>M. A. Seo, H. R. Park, S. M. Koo, D. J. Park, J. H. Kang, O. K. Suwal, S. S. Choi, P. C. M. Planken, G. S. Park, N. K. Park, Q. H. Park, and D. S. Kim, *Nature Photon.* **3**, 152 (2009).  
<sup>21</sup>H. R. Park, Y. M. Park, H. S. Kim, J. S. Kyoung, M. A. Seo, D. J. Park, Y. H. Ahn, K. J. Ahn, and D. S. Kim, *Appl. Phys. Lett.* **96**, 121106 (2010).  
<sup>22</sup>M. Shalaby, H. Merbold, M. Peccianti, L. Razzari, G. Sharma, T. Ozaki, R. Morandotti, T. Feurer, A. Weber, L. Heyderman, B. Patterson, and H. Sigg, *Appl. Phys. Lett.* **99**, 041110 (2011).  
<sup>23</sup>H.-R. Park, K. J. Ahn, S. Han, Y.-M. Bahk, N. Park, and D.-S. Kim, *Nano Lett.* **13**, 1782 (2013).  
<sup>24</sup>J. Kyoung, M. Seo, H. Park, S. Koo, H.-S. Kim, Y. Park, B.-J. Kim, K. Ahn, N. Park, H.-T. Kim, and D.-S. Kim, *Opt. Express* **18**, 16452 (2010).  
<sup>25</sup>Y. M. Bahk, H. R. Park, K. J. Ahn, H. S. Kim, Y. H. Ahn, D.-S. Kim, J. Bravo-Abad, L. Martin-Moreno, and F. J. Garcia-Vidal, *Phys. Rev. Lett.* **106**, 013902 (2011).  
<sup>26</sup>H. Shichijo and K. Hess, *Phys. Rev. B* **23**, 4197 (1981).  
<sup>27</sup>M. V. Fischetti and S. E. Laux, *Phys. Rev. B* **38**, 9721 (1988).  
<sup>28</sup>A. Di Carlo, P. Vogl, and W. Pötz, *Phys. Rev. B* **50**, 8358 (1994).